DOI: 10.31534/engmod.2023.1.ri.03v
Original scientific paper
Received: 3.04.2022.

Acoustic Analysis of Multi-Frequency Problems Using the Boundary Element Method Based on Taylor Expansion

Juan Zhao[1*], Leilei Chen[1,2,3], Haozhi Li[1], Zhongwang Wang[3,4], Wenqiang Ma[1], Xiuyun Chen[3,4]

[1] *College of Architecture and Civil Engineering, Xinyang Normal University, Xinyang, 464000, Henan, PR CHINA*

[2] *College of Intelligent Construction, Wuchang University of Technology, Wuhan, 430223, Hubei, PR CHINA*

[3] *School of Architectural Engineering, Huanghuai University, Zhumadian 463003, Henan, Henan, PR CHINA*

[4] *Henan International Joint Laboratory of Structural Mechanics and Computational Simulation, Huanghuai University, Zhumadian, 463003, PR CHINA*

[*] *the Corresponding Author: zhn19950216@126.com*

SUMMARY

This work proposes a refreshing technique that utilizes the Taylor expansion to improve the computational efficiency of the multi-frequency acoustic scattering problem. The Helmholtz equation in acoustic problems is solved using the boundary element method (BEM). In this work, the Taylor expansion is utilized to separate frequency-dependent terms from the integrand function in the boundary integral equation so that the wave number is independent of the equation system, thereby avoiding the time-consuming frequency sweep analysis. To conquer the non-uniqueness of the solution for the external acoustic field problem, the Burton-Miller method is used to linearly combine the conventional boundary integral equation and the hypersingular boundary integral equation. Moreover, to eliminate the computational difficulties caused by the Burton-Miller method, the Cauchy principal value and the Hadamard finite part integral method are used to solve singular integrals. Two-dimensional numerical examples are exploited to verify the effectiveness and compatibility of the algorithm for the multi-frequency analysis.

KEYWORDS: *acoustic analysis; boundary element method; Taylor expansion; Burton-Miller method; frequency sweep.*

1. INTRODUCTION

With the development of economic construction, urban road traffic is becoming more and more developed, and the number of car users is also increasing, therefore, road traffic noise pollution is becoming more and more serious [1-3]. Any acoustic system has three main links, namely the sound source, the transmission route, and the receiver [4]. However, in practical applications,

the more effective noise control method is usually considered from two aspects, that of the noise source and that of the noise propagation path. Although the control of noise source is the most fundamental measure, it has higher technical and economic requirements, while it is convenient and economical to set up a sound barrier on the transmission path to block the propagation of noise. As a result, the use of sound barriers to protect sensitive points near sound sources is an important measure in solving noise pollution [5-7]. The performance of the sound barrier is evaluated by many scholars using various numerical methods [8-13]. Among these numerical methods, the boundary element method (BEM) has a better application value than the finite element method (FEM) in the acoustic analysis due to its high accuracy, dimensionality reduction, and easy mesh generation [14-18]. In addition, for the external acoustic field, the Sommerfeld radiation conditions at infinity are automatically satisfied [19-21]. Engineering acoustic problems are often unbounded, and the BEM can automatically transform the infinite domain problem into a finite domain problem on the boundary. Therefore, BEM has always been an extremely important numerical method in acoustic analysis [22-25] and is selected for the acoustic analysis of two-dimensional problems in this work.

To observe the level of noise in noise control engineering, it is usually necessary to evaluate the response function over a broadband range [26]. However, the *n-th* order Hankel function of the first kind $H_n^{(1)}(kr)$ appears in the Green function for two dimensions Helmholtz equation, thereby, the coefficient matrix is related to the wave number *k*. Moreover, due to the frequency dependence of the boundary element coefficient matrix, all components in the traditional boundary element coefficient matrix must be recalculated at each different frequency. Since building the matrix requires a large number of numerical integrations, the recalculation process would cause a waste of time if a large number of individual frequency points need to be solved. Consequently, the attractiveness of the BEM decreases slightly when performing broadband analysis [27]. To circumvent this gap, some techniques have been proposed to solve multi-frequency problems, such as the fast multipole methods(FMM) [28], the frequency interpolation technique [29], the Green function interpolation technique [30], the frequency interpolation transfer function [31], the matrix interpolation and solution iterative calculation [32], the frequency response function approximation method [33] and the basic solution exponential term approximation technique [26,34]. Based on the approximation method of the basic solution exponential term, this work proposes a novel method for multi-frequency acoustic analysis. The method only performs Taylor expansion on the Hankel function in the Green function to obtain a frequency-independent matrix of boundary element coefficients. Furthermore, this method does not require a large number of numerical integrations, which reduces the amount of calculation and saves integration time.

On the other hand, the use of the single Helmholtz boundary integral equation may have the trouble of non-uniqueness of solution. To circumvent the non-uniqueness of the solution in the external sound field analysis, the Burton-Miller method [35] is used to combine the conventional boundary integral equation (CBIE) and the hypersingular boundary integral equation (HBIE) for acoustic analysis. However, using this method introduces singular integrals, which makes the calculation more difficult. This is another inherent gap in the BEM. Numerous scholars have conducted in-depth research on this problem [36-39]. Guiggiani et al. [40] proposed a general treatment of strong singular and hypersingular integrals of higher-order surface elements in 1992, which is suitable for any order element type. Subsequently, Rego Silva [41] applied the method to the acoustic BEM, which is often referred to as the singular extinction technique or the Guiggiani method. The method proposed by Guiggiani was improved by Rong et al. [42] to improve the integration accuracy when the element is distorted. Keuchel et al. [43] introduced the Guiggiani

method into the isogeometric analysis (IGA) to deal with strong singulars and hypersingular integrals in the isogeometric BEM. Chen et al. [44] utilized the Guiggiani method to process singular integrals in structural shape optimization based on the acoustic BEM. All of this work demonstrates the robust viability of the Guiggiani approach and its versatility for any type of element. The regularization method is another method to deal with singular integrals, which has a lot of representative work [45-47]. Liu et al. [45] built a system of equations of the weakly singular form of the hypersingular boundary equation based on the regularization method and certain integral identities of the static Green function. Matsumoto et al. [46] derived a set of equations of no singular boundary integration based on the discretization of triangular normal elements, which is very convenient to implement. However, the regularization method is more cumbersome and the implementation process is more complex, thereby singular integrals are directly and explicitly solved using the Cauchy principal value and the Hadamard finite partial integral method in this work.

The remainder of the paper is organized as follows. The BEM for 2D acoustic problems is given in Section 2. Frequency decoupling techniques based on Taylor theory are used to accelerate the solution of the BEM for broadband analysis in Section 3, and Section 4 describes in detail the processing of singular integrals. Section 5 includes various numerical examples used to validate the proposed acceleration algorithms process, followed by the conclusions in Section 6.

2. BEM FOR 2D ACOUSTIC PROBLEMS

The acoustic problem is governed by the following Helmholtz equation:

$$\nabla^2 p(x)+k^2 p(x)=0,\ \forall x\in \Omega \tag{1}$$

where ∇^2 is the Laplace operator, *p(x)* is the sound pressure, *k* is the wave number. The CBIE and HBIE in 2D acoustic problems are expressed respectively, as:

$$C(x)\,p(x)+\int_\Gamma F(x,y)p(y)dS(y)=\int_\Gamma G(x,y)q(y)dS(y)+p_{inc}(x), \tag{2}$$

and:

$$C(x)q(x)+\int_\Gamma H(x,y)p(y)dS(y)=\int_\Gamma K(x,y)q(y)dS(y)+\frac{\partial p_{inc}(x)}{\partial n(x)}, \tag{3}$$

where the coefficient *C(x) = 1/2* if the source point *x* lies on a smooth boundary *S*, p_{inc} *(x)* is the incident sound pressure by the plane wave or point sound source, *q(x)* represents the derivative of sound pressure *p(x)*. The expression of the kernel functions presented in the CBIE and HBIE are as follows:

$$\begin{aligned}
&G(x,y)=\frac{i}{4}H_0^{(1)}(kr),\\
&F(x,y)=\frac{\partial G(x,y)}{\partial n(y)}=-\frac{i}{4}H_1^{(1)}(kr)\frac{\partial r}{\partial n(y)},\\
&K(x,y)=\frac{\partial G(x,y)}{\partial n(x)}=-\frac{i}{4}H_1^{(1)}(kr)\frac{\partial r}{\partial n(x)},\\
&H(x,y)=\frac{\partial^2 G(x,y)}{\partial n(x)\partial n(y)}=\frac{ik}{4r}H_1^{(1)}(kr)n_j(x)n_j(y)-\frac{ik^2}{4}H_2^{(1)}(kr)\frac{\partial r}{\partial n(x)}\frac{\partial r}{\partial n(y)},
\end{aligned} \tag{4}$$

where $r = |x - y|$.

The Burton-Miller formulation [48,49] obtained by combining the CBIE and HBIE can be used to overcome the nonunique solution problem at a series of fictitious eigenfrequencies. The linear combination formulation of CBIE and HBIE is expressed as:

$$\begin{aligned} &C(x)(p(x)+\alpha q(x))+\int_S F(x,y)p(y)dS(y)+\alpha\int_S H(x,y)p(y)dS(y)= \\ &\int_S G(x,y)q(y)dS(y)+\alpha\int_S K(x,y)q(y)dS(y)+\left[p_{inc}(x)+\alpha\frac{\partial p_{inc}(x)}{\partial n(x)}\right], \end{aligned} \tag{5}$$

where α is the coupling constant [35]. For our formulations, the coupling constant that can be chosen as $-i/k$.

It is easy to notice that the kernel functions and their normal derivative in the above equation are singular. Thus, to accurately tackle singular integrals, the Cauchy principal value and the Hadamard finite part integral method are utilized in this work, as detailed in Section 4.

In this work, we use the constant element to discretize the boundary of the structure. After the discretization of Eq. (5), we can obtain the following matrix form:

$$\boldsymbol{Hp}=\boldsymbol{Gq}+\boldsymbol{p}_{inc}, \tag{6}$$

where the coefficient matrices $\boldsymbol{H}$ and $\boldsymbol{G}$ of the BEM are fully populated, asymmetric and frequency-dependent. Introducing the boundary condition, we can obtain the following linear system of the equation:

$$\boldsymbol{Az}=\boldsymbol{b}, \tag{7}$$

where $\boldsymbol{A}$ is the coefficient matrix, $\boldsymbol{z}$ is the unknown vector containing sound pressure or its normal derivative at the nodes, and $\boldsymbol{b}$ is the known vector. By solving Eq. (7), we can obtain the unknown vector $\boldsymbol{z}$. Therefore, using Eq. (2) with *C(x)=1*, we obtain the sound pressure vector at several points lying on the acoustic domain, as follows:

$$\boldsymbol{p}_f=\boldsymbol{G}_f\boldsymbol{q}-\boldsymbol{H}_f\boldsymbol{p}+\boldsymbol{p}_f^{inc}, \tag{8}$$

where $\boldsymbol{H}_f$ and $\boldsymbol{G}_f$ are the coefficient matrices with $x\in\Omega$.

3. FREQUENCY DECOUPLING BASED ON TAYLOR THEORY

We carry out Taylor expansion [50-52] of the *n-th* order Hankel function of the first kind at the fixed point z_0, as follows:

$$H_n^{(1)}(z)=\sum_{m=0}^{\infty}\frac{(z-z_0)^m}{m!}\left[H_n^{(1)}(z)\right]_{z=z_0}^{(m)}, \tag{9}$$

where:

$$\left[H_n^{(1)}(z)\right]_{z=z_0}^{(m)}=\frac{d^m H_n^{(1)}(z)}{dz^m}\Big|_{z=z_0}, \tag{10}$$

By replacing z and z_0 with kr and kr_0 respectively, we can obtain the expansion expressions of the Hankel function in Eq. (4). It is worth noting that obtaining an explicit expression of the *m-th* order derivative of the *n-th* order Hankel function is very difficult. The recursive expression of the Hankel function is expressed as:

$$\frac{dH_n^{(1)}(z)}{dz}=\frac{n}{z}H_n^{(1)}(z)-H_{n+1}^{(1)}(z). \tag{11}$$

By differentiating Eq. (11) with respect to variable x repeatedly, we can obtain the recursive expression of the *m-th* order derivative of the *n-th* order Hankel function, as follows:

$$\left[H_n^{(1)}(z)\right]^{(m)}=\sum_{i=1}^{m}\left[H_n^{(1)}(z)\right]^{(m-i)}\frac{(-1)^{i+1}(m-1)!}{z^i(m-i)!}-\left[H_{n+1}^{(1)}(z)\right]^{(m-1)}, \tag{12}$$

By substituting Eq. (12) into Eq. (9) and replacing z and z_0 with kr and kr_0, we can obtain the solution of expansion expression of $H_n^{(1)}(kr)$ at the fixed frequency point k_0.

In this work, the impedance boundary condition $q(x)=ik\beta p(x)$ is introduced to simulate the sound-absorption characteristics. Thus, the integrals in the Burton-Miller formulation can be rewritten as a form of Taylor expansion at the fixed frequency point k_0:

$$\begin{aligned}
&\int_S F(x,y)p(y)dS(y)=\sum_{m=0}^{\infty}\frac{(k-k_0)^m}{m!}I_1^m,\\
&\int_S G(x,y)q(y)dS(y)=\sum_{m=0}^{\infty}\frac{(k-k_0)^m}{m!}kI_2^m,\\
&\alpha\int_S H(x,y)p(y)dS(y)=\sum_{m=0}^{\infty}\frac{(k-k_0)^m}{m!}(kI_3^m+k^2I_4^m),\\
&\alpha\int_S K(x,y)q(y)dS(y)=\sum_{m=0}^{\infty}\frac{(k-k_0)^m}{m!}k^2I_5^m,
\end{aligned} \tag{13}$$

where I_1^m, I_2^m, I_3^m, I_4^m, and I_5^m are expressed, respectively, as:

$$\begin{aligned}
I_1^m&=-\int_S\frac{ir^{m-1}}{4}\left[zH_1^{(1)}(z)\right]_{z=k_0r}^{(m)}\frac{\partial r}{\partial n(y)}p(y)dS(y),\\
I_2^m&=-\int_S\frac{\beta r^m}{4}\left[H_0^{(1)}(z)\right]_{z=k_0r}^{(m)}p(y)dS(y),\\
I_3^m&=\int_S\frac{\alpha ir^{m-1}}{4}\left[H_1^{(1)}(z)\right]_{z=k_0r}^{(m)}n_j(x)n_j(y)p(y)dS(y),\\
I_4^m&=\int_S\frac{\alpha ir^m}{4}\left[H_2^{(1)}(z)\right]_{z=k_0r}^{(m)}\frac{\partial r}{\partial n(x)}\frac{\partial r}{\partial n(y)}p(y)dS(y),\\
I_5^m&=\int_S\frac{\alpha\beta r^m}{4}\left[H_1^{(1)}(z)\right]_{z=k_0r}^{(m)}\frac{\partial r}{\partial n(x)}p(y)dS(y).
\end{aligned} \tag{14}$$

The *m-th* derivative of $zH_1^{(1)}(z)$ function used for solution of I_1^m integral in Eq. (14) is derived as:

$$\left[zH_1^{(1)}(z)\right]^{(m)}=m\left[H_1^{(1)}(z)\right]^{(m-1)}+z\left[H_1^{(1)}(z)\right]^{(m)}. \tag{15}$$

By substituting Eq. (13) into the Burton-Miller formulation with the impedance boundary condition, the expression of the Burton-Miller formulation can be reformulated as follows:

$$C(x)p(x)(1+\alpha ik\beta)+\sum_{m=0}^{\infty}\frac{(k-k_0)^m}{m!}\left[I_1^m+k(-I_2^m+I_3^m)+k^2(I_4^m-I_5^m)\right] =\left[p_{inc}(x)+\alpha\frac{\partial p_{inc}(x)}{\partial n(x)}\right]. \tag{16}$$

By discretizing Eq. (16), we obtain the following matrix form as:

$$\boldsymbol{C}\boldsymbol{p}+k\bar{\boldsymbol{C}}\boldsymbol{p}+\sum_{m=0}^{\infty}\frac{(k-k_0)^m}{m!}[\boldsymbol{I}_1^m+k\boldsymbol{I}_2^m+k^2\boldsymbol{I}_3^m]\boldsymbol{p}=\boldsymbol{P}_{inc}, \tag{17}$$

where:

$$\boldsymbol{C}=\begin{bmatrix} c_1 & & 0 \\ & \ddots & \\ 0 & & c_N \end{bmatrix}, \tag{18}$$

and:

$$\bar{\boldsymbol{C}}=\alpha i\begin{bmatrix} \beta_1 c_1 & & 0 \\ & \ddots & \\ 0 & & \beta_N c_N \end{bmatrix}. \tag{19}$$

We construct new matrices, as follows:

$$\tilde{\boldsymbol{I}}_1^m=\begin{cases}\boldsymbol{C}+\boldsymbol{I}_1^0, & m=0\\ \boldsymbol{I}_1^m, & m\neq 0\end{cases}, \tag{20}$$

and:

$$\tilde{\boldsymbol{I}}_2^m=\begin{cases}\bar{\boldsymbol{C}}+\boldsymbol{I}_2^0, & m=0\\ \boldsymbol{I}_2^m, & m\neq 0\end{cases}. \tag{21}$$

Using Eq. (20) and Eq. (21) and setting $\boldsymbol{I}_3^m=\tilde{\boldsymbol{I}}_3^m$, Eq. (17) can be rewritten as:

$$\left[\sum_{m=0}^{\infty}\frac{(k-k_0)^m}{m!}\left(\tilde{\boldsymbol{I}}_1^m+k\tilde{\boldsymbol{I}}_2^m+k^2\tilde{\boldsymbol{I}}_3^m\right)\right]\boldsymbol{p}=\tilde{\boldsymbol{P}}_{inc}, \tag{22}$$

In this work, we can decompose the frequency-dependent system matrix in Eq. (6) into the sum of the frequency-dependent scalar function multiplied by the frequency-independent system matrix using the Taylor expansion technique. According to Eq. (14), it is easy to notice that the coefficients $\tilde{\boldsymbol{I}}_1^m$, $\tilde{\boldsymbol{I}}_2^m$, and $\tilde{\boldsymbol{I}}_3^m$ are not frequency-dependence and need only be computed once for multi-frequency problems. Therefore, the coefficient matrix is not frequency-dependent.

4. SINGULAR INTEGRAL PROCESSING

The boundary integrals for Green functions in Eq. (14) normally can be rewritten as:

$$\int_S f(y)dS(y)=\underbrace{\int_{S\setminus S_x} f(y)dS(y)}_{nonsingular}+\underbrace{\int_{S_x} f(y)dS(y)}_{singular}, \tag{23}$$

where $S \setminus S_x$ denotes the boundary S except S_x, S_x is the element containing the source point x. The integrals in $S \setminus S_x$ are nonsingular and the Gaussian integration method can be used to solve them effectively. However, singular integrals exist in S_x, and special handing needs to be carried out for solving the singular integrals. Actually, only I_2^m and I_3^m contain singular integral term because of $\frac{\partial r}{\partial n(x)} = \frac{\partial r}{\partial n(y)} = 0$, for $y \in S_x$.

In this work, the Cauchy principal value and the Hadamard finite part integral method are utilized to evaluate explicitly and directly the singular integrals [28,53], as shown in Figure 1. S_ε is a semi-circle with a radius ε and Γ_ε is $S_x \setminus S_\varepsilon$. Thus, the singular term in Eq. (23) can be rewritten as:

$$\int_{S_x} f(y)dS(y) = \lim_{\varepsilon \to 0}\left(\int_{\Gamma_\varepsilon} f(y)dS(y) + \int_{S_\varepsilon} f(y)dS(y) \right), \tag{24}$$

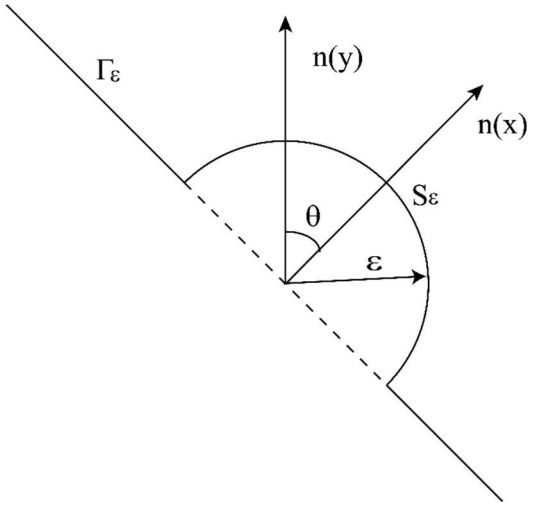

Fig. 1 *An infinitesimal hemicircle attached to the constant element* S_x

Suppose that the singular term of the function *f(y)* is *D(y)*. By eliminating the singular part, Eq. (24) can be reformulated in the following form:

$$\int_{S_x} f(y)dS(y) = \underbrace{\lim_{\varepsilon \to 0} \int_{\Gamma_\varepsilon} [f(y) - D(y)]dS(y)}_{nonsingular} + \underbrace{\lim_{\varepsilon \to 0} \int_{S_\varepsilon} f(y)dS(y)}_{singular} + \underbrace{\lim_{\varepsilon \to 0} \int_{\Gamma_\varepsilon} D(y)dS(y)}_{singular}. \tag{25}$$

By replacing the integral terms of I_2^m and I_3^m with f_2^m and f_3^m respectively, we obtain the following formulas:

$$\begin{aligned} f_2^m &= r^m \left[H_0^{(1)}(z) \right]_{z=k_0 r}^{(m)}, \\ f_3^m &= r^{m-1} \left[H_1^{(1)}(z) \right]_{z=k_0 r}^{(m)}, \end{aligned} \tag{26}$$

Using Eq. (25), we can obtain the solution of I_2^m and I_3^m in S_x, as follows:

$$\begin{aligned}\int_{S_x} f_2^m dS(y) &= \underbrace{\lim_{\varepsilon\to 0}\int_{\Gamma_\varepsilon}\left[f_2^m - D_2^m\right]dr}_{nonsingular} + \underbrace{\lim_{\varepsilon\to 0}\left\{\left[-2rD_2^m\right]_{r=\varepsilon}\right\}}_{g_2^m} + \underbrace{\lim_{\varepsilon\to 0}\int_{\Gamma_\varepsilon} D_2^m dr}_{d_2^m},\\ \int_{S_x} f_3^m dS(y) &= \underbrace{\lim_{\varepsilon\to 0}\int_{\Gamma_\varepsilon}\left[f_3^m - D_3^m\right]dr}_{nonsingular} + \underbrace{\lim_{\varepsilon\to 0}\left\{\left[-2rD_3^m\right]_{r=\varepsilon}\right\}}_{g_3^m} + \underbrace{\lim_{\varepsilon\to 0}\int_{\Gamma_\varepsilon} D_3^m dr}_{d_3^m},\end{aligned} \tag{27}$$

where $dr = dS(y)$ and $n_j(x)n_j(y) = 1$ in S_x. For nonsingular terms, the Gaussian integration method is used for the solution of integrals. However, for singular terms, we still need to obtain the expression of singular parts D_2^m and D_3^m.

The singular part of $H_0^{(1)}(z)$ is $2i\ln(z)/\pi$, and the singular part of $H_1^{(1)}(z)$ is $2i/(-\pi z) + iz\ln(z)/\pi$. By differentiating the two singular parts repeatedly, the singular parts D_2^m and D_3^m of f_2^m and f_3^m integrals can be derived as:

$$D_2^m = \begin{cases} \dfrac{2i}{\pi}\ln(k_0 r), & m = 0 \\ O(r^0), & m \neq 0 \end{cases}, \tag{28}$$

and:

$$D_3^m = \begin{cases} -\dfrac{2i}{\pi}k_0^{-1}r^{-2} + \dfrac{ik_0}{\pi}\ln(k_0 r), & m = 0 \\ \dfrac{2i}{\pi}k_0^{-2}r^{-2} + \dfrac{i}{\pi}\ln(k_0 r), & m = 1 \\ -\dfrac{2i}{\pi}(-1)^m k_0^{-(m+1)}r^{-2}m!, & m \geq 2 \end{cases}, \tag{29}$$

By investigating Eq. (28), we can see that the term f_2^m is weakly singular for *m=0*, otherwise nonsingular. However, the term f_3^m is hypersingular. By bringing Eq. (28) into the first formulation in Eq. (27), the expressions of g_2^0 and d_2^0 can be derived as:

$$\begin{aligned} g_2^0 &= 0, \\ d_2^0 &= \frac{2iL}{\pi}\left[\ln(k_0 L/2) - 1\right], \end{aligned} \tag{30}$$

where *L* is the length of the element.

By bringing Eq. (29) into the second formulation in Eq. (27), the expressions of g_3^m and d_3^m can be derived as:

$$g_3^m = \lim_{\varepsilon\to 0}\left[\frac{4i}{\pi}(-1)^m k_0^{-(m+1)}m!\frac{1}{\varepsilon}\right], \tag{31}$$

and:

$$d_3^m = \begin{cases} \dfrac{8i}{\pi k_0 L} + \dfrac{ik_0 L}{\pi}\left[\ln(k_0 L/2) - 1\right] - \lim\limits_{\varepsilon \to 0} \dfrac{4i}{\pi k_0 \varepsilon}, & m = 0 \\ \dfrac{-8i}{\pi k_0^2 L} + \dfrac{iL}{\pi}\left[\ln(k_0 L/2) - 1\right] + \lim\limits_{\varepsilon \to 0} \dfrac{4i}{\pi k_0^2 \varepsilon}, & m = 1. \\ \dfrac{8i}{\pi L}(-1)^m k_0^{-(m+1)} m! - \lim\limits_{\varepsilon \to 0}\left[\dfrac{4i}{\pi}(-1)^m k_0^{-(m+1)} m! \dfrac{1}{\varepsilon}\right], & m \geq 2 \end{cases} \quad (32)$$

5. NUMERICAL EXAMPLES

In this work, two numerical examples are utilized to investigate the accuracy of the Taylor expansion algorithm. The computation is implemented in a Fortran 90 self-programming program and carried out on a desktop computer with 4GB of RAM and an Intel Core i5 CPU. OpenMP technology is used for parallel computing to improve computing efficiency, and the parallel parameter is 6. The parallel parameter here refers to the number of parallel threads. In this section, 10 Gaussian quadrature points are utilized to solve singular integrals, and only 6 Gaussian quadrature points are required for non-singular integrals.

5.1 ACOUSTIC SCATTERING FROM AN INFINITELY LONG RIGID CYLINDER

The scatterer of the acoustic scattering problem is an infinitely long rigid cylinder with Neumann boundary conditions, which can be simplified to a circle as shown in Figure 2. The incident direction of the incident plane wave is parallel to the positive direction of the x - axis. The radius r_0 of the circle is *1 m* and the center of the circle is at (*0 m, 0 m*). The circle is divided into 300 elements using the constant boundary element, and the observation point is at the point (*2 m, 0 m*). The remaining parameters are shown in Table 1.

Table 1 *Related parameters of the circle*

The density of the air medium	ρ_f	*1.21*	*kg/m³*
The speed of the sound	c_{air}	*343*	*m/s*
The frequency step	f_{step}	*1.0*	*Hz*

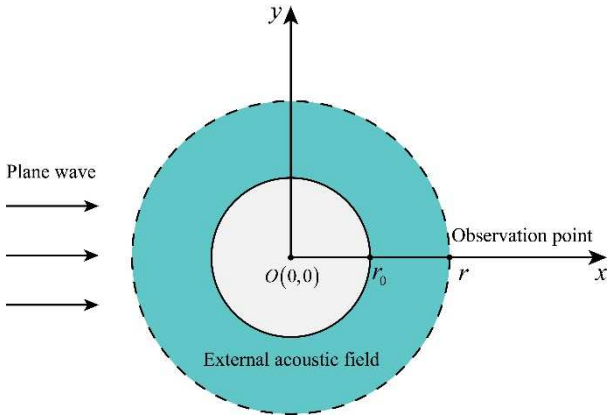

Fig. 2 *Acoustic scattering from an infinitely long rigid cylinder with a radius of r_0*

Subsequently, the sound pressure p_{inc} of the incident plane wave is defined as:

$$p_{inc} = p_0 e^{ikr\cos\theta}, \tag{33}$$

where $p_0=1$ is the amplitude of the incident plane wave, θ is 0 because the incident wave propagates in the forward direction along the x - axis. The analytical expression [54] for the distribution of the scattering sound field of the infinitely long rigid cylinder is as follows

$$p(r,\theta) = -\sum_{n=0}^{\infty} \varepsilon_n i^n \frac{nJ_n(kr_0) - kr_0 J_{n+1}(kr_0)}{nH_n^{(1)}(kr_0) - kr_0 H_{n+1}^{(1)}(kr_0)} H_n^{(1)}(kr)\cos(n\theta) \tag{34}$$

where the number of the truncated term is 50. ε_n denotes the Neumann symbol, $\varepsilon_0 = 1$ for $n = 0$, while $\varepsilon_n = 2$ for $n > 0$.

Relative errors in the L_2-norm form are expressed as follows:

$$e^{\Gamma} = \left(\sum_{i=1}^{N} \left| p_n(x_i) - p_e(x_i) \right|^2 \right)^{1/2} \Bigg/ \left(\sum_{i=1}^{N} \left| p_e(x_i) \right|^2 \right)^{1/2}, \tag{35}$$

where $p_e(x_i)$ represents the exact solution for the sound pressure at the point in the domain, $p_n(x_i)$ represents the numerical solution of sound pressure, x_i is the position of the calculation point in the domain, N is the number of calculated points. This subsection takes 360 points evenly distributed on the boundary of the circle with a radius of *2 m* in Figure 2 as reference points for error calculation.

Firstly, the comparison of the numerical solution based on Taylor expansion with the analytical solution at the observation point (*2 m, 0 m*) is shown in Figure 3. The sound pressure results are solved using the BEM based on Taylor expansion in four frequency ranges, such as [*2, 50*] *Hz,* [*50, 100*] *Hz*, [*100, 150*] *Hz* and [*150, 200*] *Hz*. In this work, the frequency step is *1 Hz* and the fixed frequency expansion point k_0 in the frequency range $\left[f_{low}, f_{up} \right]$ is assumed to be $(f_{low} + f_{up})/2$. Herein, "Taylor_3" represents the numerical solution obtained using BEM based on Taylor expansion with TM=3 expansion terms. Likewise, "Taylor_5", "Taylor_7" and "Taylor_10" represent the numerical solution with TM=5, 7, 10 expansion terms, respectively. It can be observed from the figure that the sound pressure values in different frequency bands are inconsistent, and the sound pressure values obtained by the numerical method and the analytical method are basically similar in the same frequency band. In addition, the expansion point is *26 Hz* within [*2, 50*] *Hz*, and the farther away from the expansion point, the greater the error. Therefore, the greater the difference in sound pressure values for different expansion terms in the [*40, 50*] *Hz* range. And the value of the "Taylor_10" is closest to the sound pressure value obtained by the analytical method, which means that the larger the Taylor expansion term, the closer the numerical solution is to the analytical solution. Further relative error analysis is shown in Figure 4. In this work, Eq. (35) is used for the relative error analysis. It can be observed from the figure that the larger the Taylor expansion term in the same frequency band, the smaller the relative error. Therefore, 10 Taylor expansion terms are utilized for the Taylor expansion in the future. The results prove the accuracy and validity of the algorithm proposed in this work.

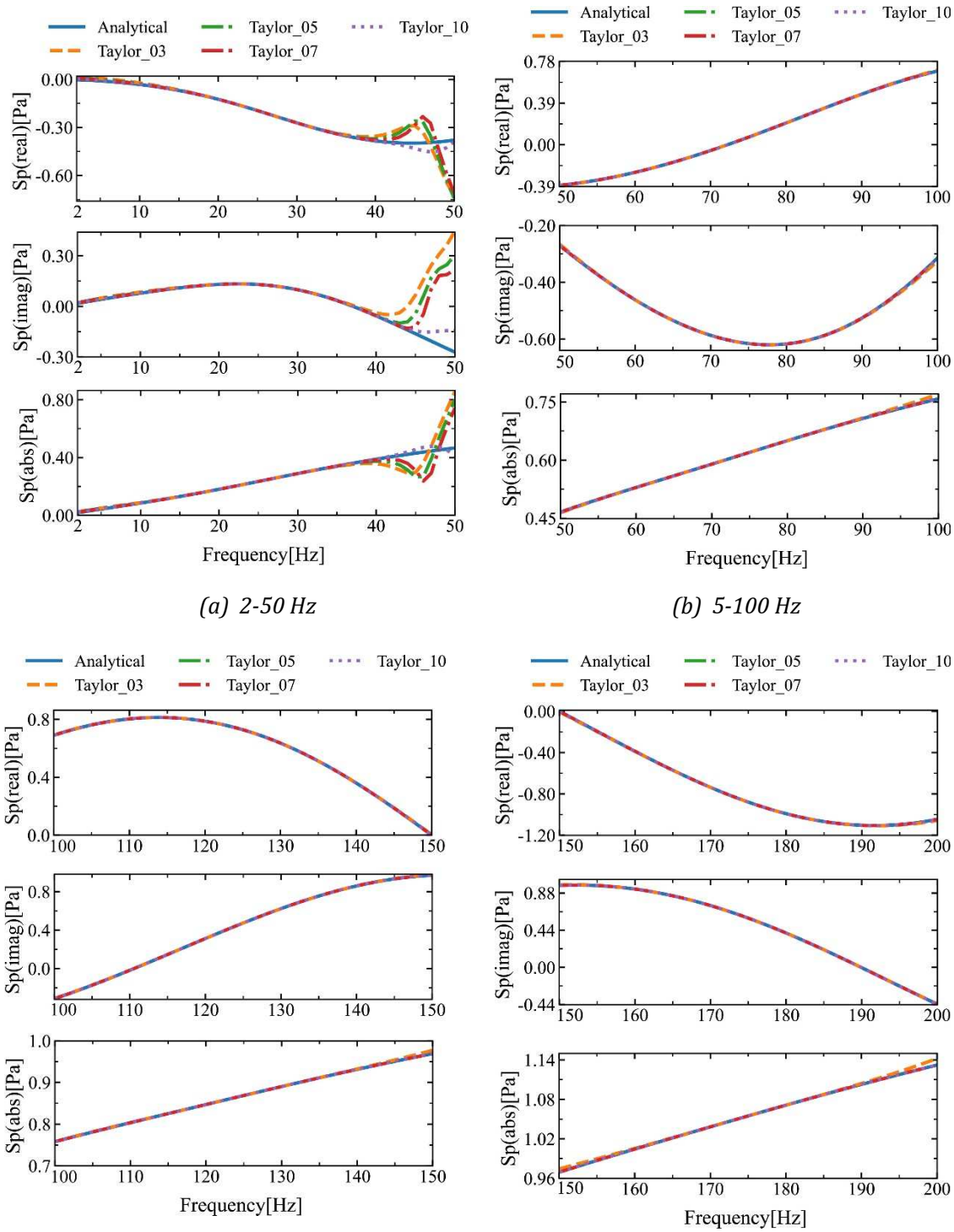

(a) 2-50 Hz *(b) 5-100 Hz*

(c) 100-150 Hz *(d) 150-200 Hz*

Fig. 3 *Relationship between sound pressure and frequency in different frequency bands obtained using the analytic method and the BEM based on Taylor expansion*

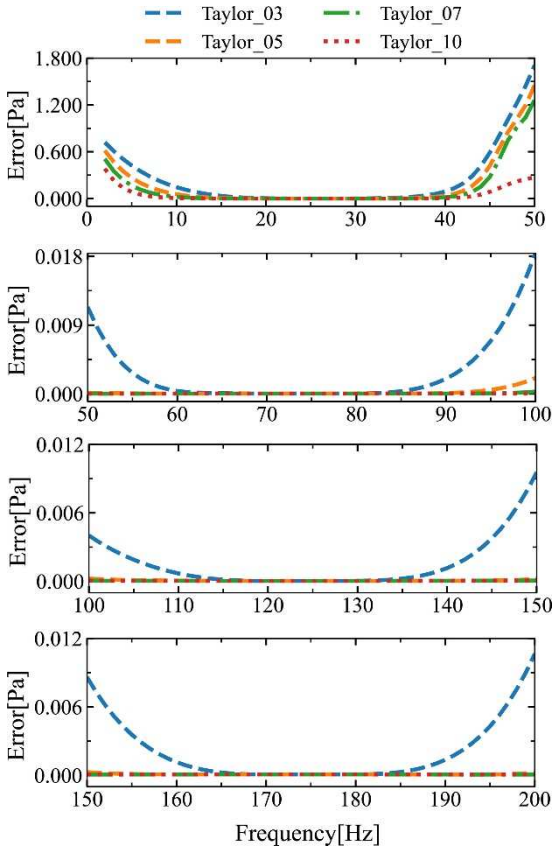

Fig. 4 *The relative error between the numerical and analytical solutions of sound pressure*

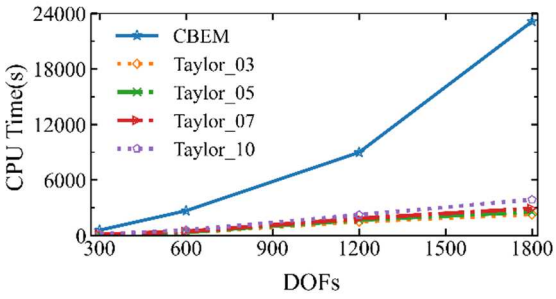

Fig. 5 *The CPU time for wideband computing in terms of DOFs*

It is necessary to investigate the CPU time used by the present algorithm and the CBEM, as shown in Figure 5. The frequency range is set to [*100, 200*] *Hz*. The number of sweeps is set to 1000. Here, "CBEM" indicates that the conventional BEM was used to solve the full-order system of equations repeatedly. From the figure, it can be observed that the CPU time required to solve the system of equations using the CBEM is significantly higher than that required using the BEM based on Taylor expansion. Thus, the decoupling method effectively reduces the computation time for wideband calculations.

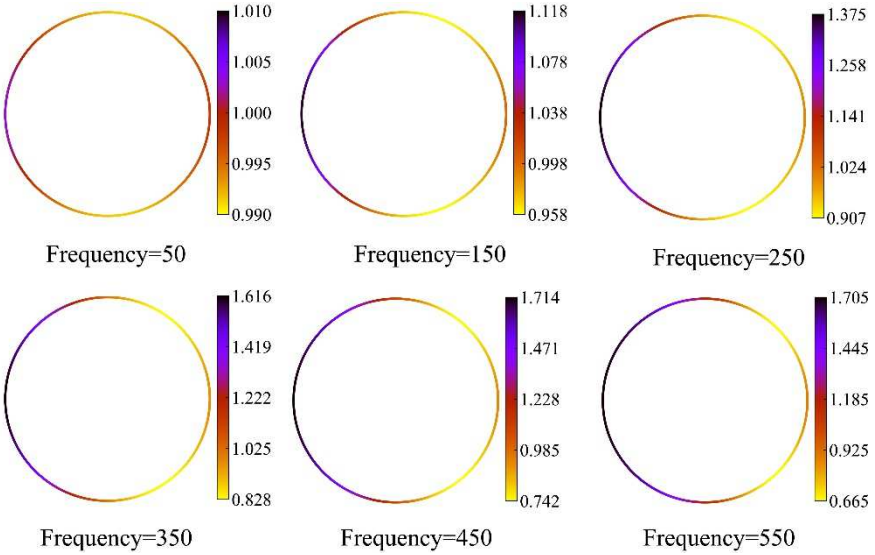

Fig. 6 *Distribution of sound pressure at different frequency points*

At six different computing frequency points of *50, 150, 250, 350, 450,* and *550 Hz*, the sound pressure at the boundary of the circle is shown in Figure 6. At the same frequency points, the contour of the sound pressure generated by the cylindrical scattering on the surface is shown in Figure 7. Herein, the sound field analysis is performed using the BEM based on Taylor expansion. For the BEM based on Taylor expansion, *25, 100, 200, 300, 400,* and *500 Hz* are considered frequency expansion points used for the solution at six different frequencies of *50, 150, 250, 350, 450,* and *550 Hz*. From the two figures, it can be seen that the sound pressure results at different frequencies are inconsistent. When performing broadband analysis, the coefficient matrix has to be repeatedly computed at every frequency point, which is very time-consuming. Therefore, it is necessary to develop efficient and fast calculation methods for frequency sweep analysis.

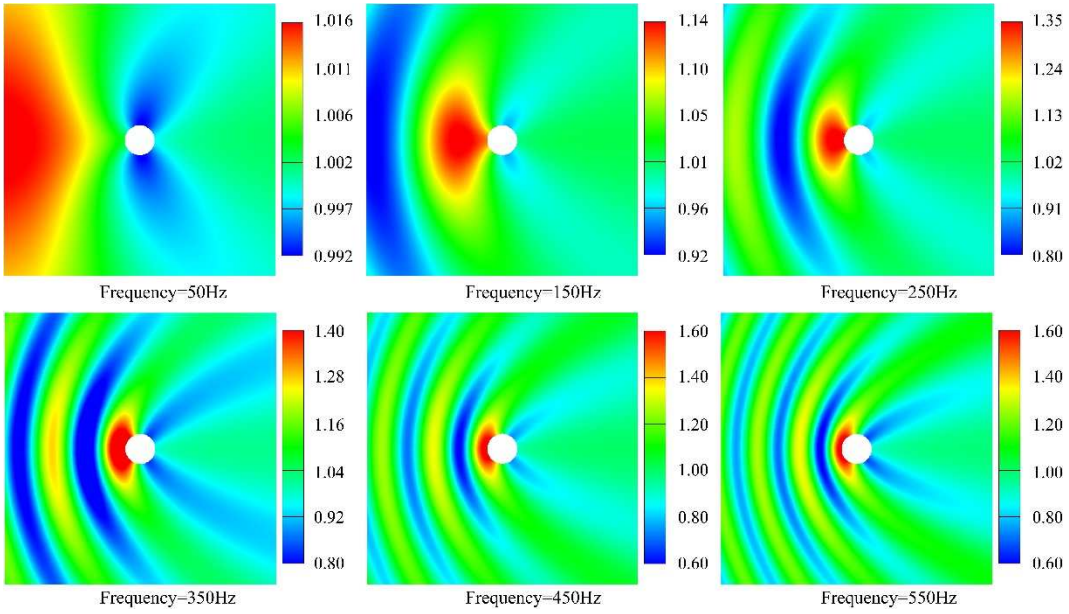

Fig. 7 *The contour of sound pressure at different frequency points*

5.2 ACOUSTIC SCATTERING FROM THE TUNING FORK-SHAPED SOUND BARRIER

With the rapid development of the economy, the number of cars has increased significantly. Although the significant increase in the number of cars has brought convenience to people, it has also brought serious traffic noise pollution on the other hand. To obtain effective noise reduction performance, there has been a gradual increase in wide use of sound barriers. Therefore, it is necessary to carry out the analysis of the noise reduction performance of the acoustic barrier.

Next, we will consider the design domain of the tuning fork-shaped sound barrier model to demonstrate the effectiveness of the proposed program in this work, as shown in Figure 8. In this subsection, we use the constant element to discretize the surface boundary of the acoustic barrier into 910 elements. A unit point sound source is set at (*0 m, 1 m*), and other related parameters are shown in Table 2. The purpose of this example is to evaluate the performance of the broadband computing algorithm based on the Taylor expansion.

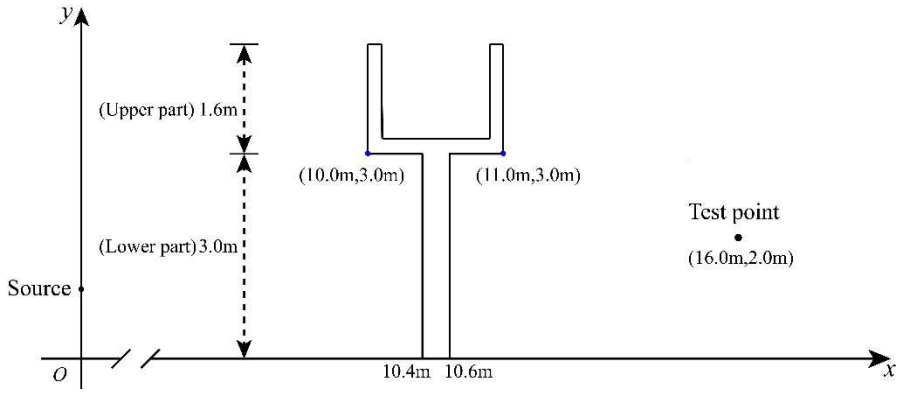

Fig. 8 *The design domain of the tuning fork-shaped sound barrier*

Table 2 *Related parameters of the sound barrier*

The density of the air medium	ρ_f	*1.21*	*kg/m³*
The speed of the sound	c_{air}	*343*	*m/s*
The thickness of the upper part of the barrier	d_1	*0.1*	*m*
The thickness of the lower part of the barrier	d_2	*0.2*	*m*

Figure 9 shows the real part of the sound pressure obtained by the BEM based on Taylor expansion at calculated points (*16 m, 2 m*). The entire frequency range of *1-300 Hz* is divided into six frequency bands, such as [*1, 50*] *Hz*, [*50, 100*] *Hz*, [*100, 150*] Hz, [*150, 200*] *Hz*, [*200, 250*] *Hz*, [*250, 300*] *Hz*. Moreover, the expansion point k_0 is located in the middle of the sub-interval, and the frequency step is set to *1 Hz*. It can be observed from the figure that the real part of the sound pressure based on Taylor expansion in different frequency bands is inconsistent. However, the sound pressure results for different expansion terms are basically consistent in the same frequency band (except in the [*1, 50*] *Hz*). This is mainly because the results of different expansion terms are frequency-dependent, and the more accurate the results become as the frequency increases. The real part of the sound pressure gradually becomes smaller as the Taylor expansion term increases within the frequency range [*1, 50*] *Hz*. In addition, the expansion point

is *25 Hz* within [*1, 50*] *Hz*, and the farther away from the expansion point, the greater the error. Therefore, the greater is the difference in sound pressure values for different expansion terms in the [*40, 50*] *Hz* range. The imaginary part and amplitude of sound pressure obtained by using BEM based on Taylor expansion at calculated points (*16 m, 2 m*) are studied in Figure 10 and Figure 11, and the variation trend is similar to Figure 9. The results also demonstrate the accuracy of the program proposed in this work.

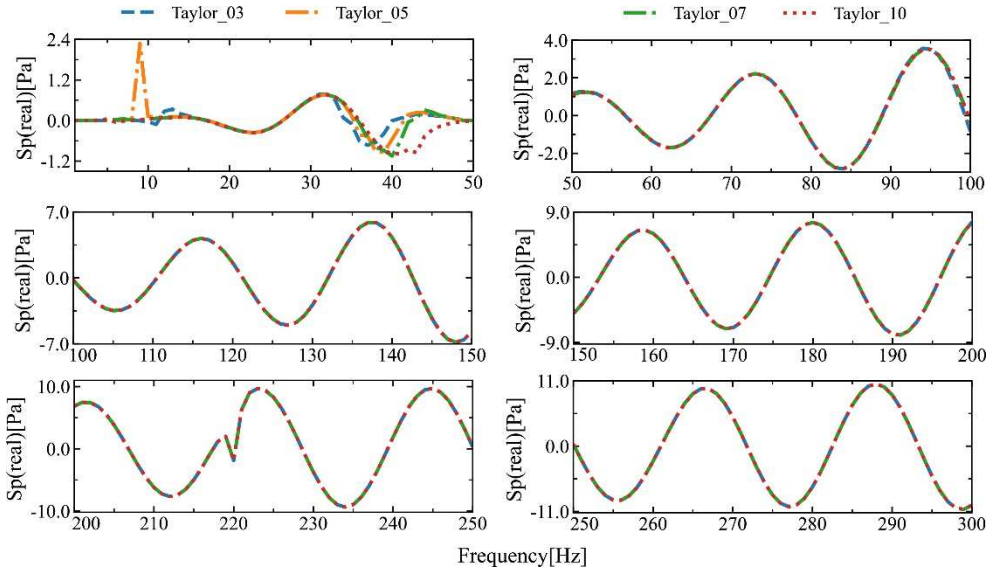

Fig. 9 *The real part of the frequency sound pressure obtained by using BEM based on Taylor expansion at calculated points (16 m, 2 m)*

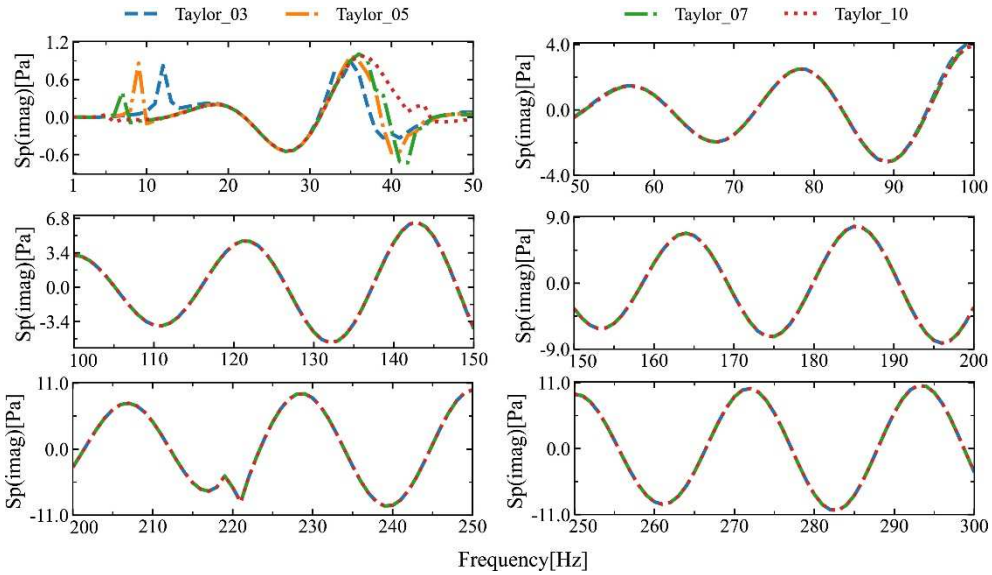

Fig. 10 *The imaginary part of the frequency sound pressure obtained by using BEM based on Taylor expansion at calculated points (16 m, 2 m)*

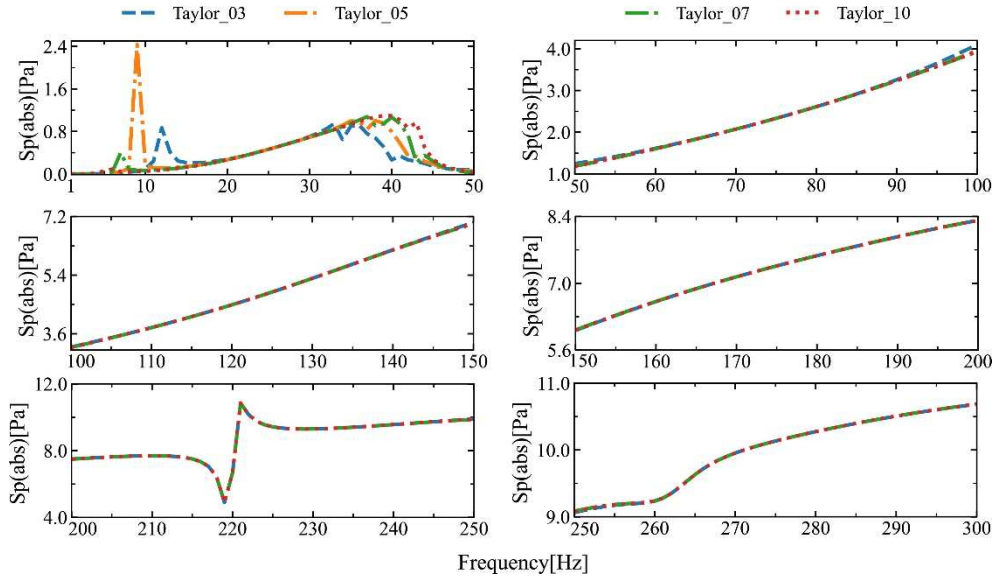

Fig. 11 *The amplitude of the frequency sound pressure obtained by using BEM based on Taylor expansion at calculated points (16 m, 2 m)*

It is worth noting from Figure 9 to Figure 11 that there is a slight deviation in the sound pressure values at *220 Hz*. Therefore, we will next compare the sound pressure values obtained using the CBEM and the BEM based on Taylor expansion in the [*200, 250*] *Hz* range, as shown in Figure 12. In Figure 12, "CBEM" denotes conventional BEM used to solve the full-order system of equations repeatedly. We can find that the sound pressure results obtained using the CBEM method and the BEM with the Taylor expansion are basically the same at *220 Hz* and around the expansion point. Thus, these results demonstrate the accuracy of the proposed algorithm.

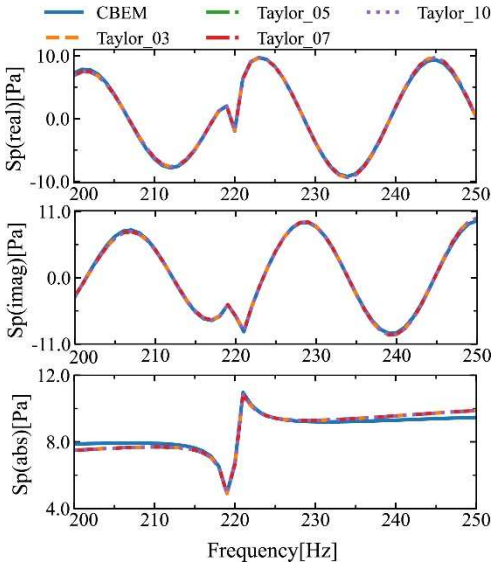

Fig. 12 *Comparison of sound pressure between the BEM based on Taylor expansion and the traditional BEM at frequency range [200,250] Hz*

It is necessary to investigate the computational efficiency of the proposed technique, as shown in Figure 13. The frequency range is set to [*100, 200*] *Hz*. Figure 13 shows the computational

time for solving the system of BEM equations at 1000 different frequencies. From the graph, it can be observed that the CPU time required to solve the system of equations using the CBEM is significantly higher than that required using the BEM based on Taylor expansion.

The Taylor expansion is used to separate the frequency variable from the Hankel function to obtain the frequency-independent coefficient matrix of boundary element. Therefore, this operation avoids the repeated calculation of the coefficient matrix, which can effectively improve computational efficiency.

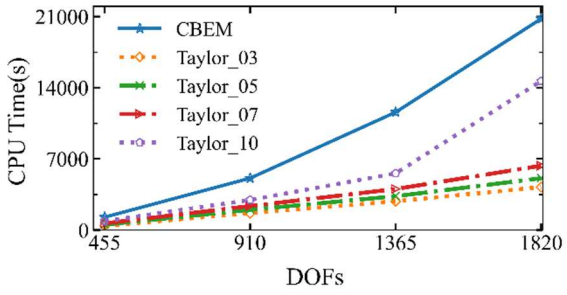

Fig. 13 *The CPU time for wideband computing in terms of DOFs*

6. CONCLUSIONS

In this work, acoustic scattering problems are analyzed using the BEM, and an accelerated computing technique is proposed. The BEM only needs to discretize the structural surface for the external acoustic field problems. In addition, the Burton-Miller formulation is utilized to eliminate virtual eigenfrequencies. The Cauchy principal value and the Hadamard finite part integral method are utilized to solve the singular integrals. This paper utilizes the Taylor expansion to separate frequency-dependent terms from the integrand function, which eliminates the frequency dependence of the boundary element coefficient matrix. Therefore, the numerical integration is restricted to the frequency-independent part, reducing the computational effort.

Although Taylor expansion overcomes the inherent drawback of frequency dependence, the order of the whole system equation is not reduced, and the state space dimension of the system equation remains unchanged. To solve this problem, we will introduce model order reduction technology (MOR) in the future.

7. AKNOWLEDGEMENT

The authors appreciate the financial support from the Postgraduate Education Reform and Quality Improvement Project of Henan Province under Grant No. YJS2022AL143.

8. REFERENCES

[1] X.Y. Wen, G.Y. Lu, K. Lv, M.J. Jin, X.F. Shi, F.H. Lu, D.Y. Zhao, Impacts of traffic noise on roadside secondary schools in a prototype large Chinese city, *Applied Acoustics*, Vol. 151, pp. 153–163, 2019. https://doi.org/10.1016/j.apacoust.2019.02.024

[2] X.D. Lu, J. Kang, P.S. Zhu, J. Cai, F. Guo, Y. Zhang, Influence of urban road characteristics on traffic noise, *Transportation Research Part D: Transport and Environment*, Vol. 75, pp. 136–

155, 2019. https://doi.org/10.1016/j.trd.2019.08.026

[3] W.J. Yang, J.Y. He, C.M. He, M. Cai, Evaluation of urban traffic noise pollution based on noise maps, *Transportation Research Part D: Transport and Environment*, Vol. 87, Article ID 102516, 2020. https://doi.org/10.1016/j.trd.2020.102516

[4] R.F. Barron, *Industrial Noise Control and Acoustics* (1st ed.), CRC Press, 2002. https://doi.org/10.1201/9780203910085

[5] R. Toledo, J.J. Aznárez, O. Maeso, D. Greiner, Optimization of thin noise barrier designs using Evolutionary Algorithms and a Dual BEM Formulation, *Journal of Sound and Vibration*, Vol. 334, pp. 219–238, 2015. https://doi.org/10.1016/j.jsv.2014.08.032

[6] W.C. Zhao, L.L. Chen, C.J. Zheng, C. Liu, H.B. Chen, Design of absorbing material distribution for sound barrier using topology optimization, *Structural and Multidisciplinary Optimization*, Vol. 56, No. 2, pp. 315–329, 2017. https://doi.org/10.1007/s00158-017-1666-8

[7] L.L. Chen, W.C. Zhao, X.H. Yuan, B.C. Zhou, Study on the Optimization of the Distribution of Absorbing Material on a Noise Barrier, *Acoustics Australia*, Vol. 46, No. 1, pp. 119–130, 2018. https://doi.org/10.1007/s40857-017-0123-6

[8] T. Ishizuka, K. Fujiwara, Performance of noise barriers with various edge shapes and acoustical conditions, *Applied Acoustics*, Vol. 65, No. 2, pp. 125–141, 2004. https://doi.org/10.1016/j.apacoust.2003.08.006

[9] M.R. Monazzam, Y.W. Lam, Performance of profiled single noise barriers covered with quadratic residue diffusers, *Applied Acoustics*, Vol. 66, No. 6, pp. 709–730, 2005. https://doi.org/10.1016/j.apacoust.2004.08.008

[10] S. Grubeša, K. Jambrošić, H. Domitrović, Noise barriers with varying cross-section optimized by genetic algorithms, *Applied Acoustics*, Vol. 73, No. 11, pp. 1129–1137, 2012. https://doi.org/10.1016/j.apacoust.2012.05.005

[11] C. Liu, L.L. Chen, W.C. Zhao, H.B. Chen, Shape optimization of sound barrier using an isogeometric fast multipole boundary element method in two dimensions, *Engineering Analysis with Boundary Elements*, Vol. 85, pp. 142–157, 2017. https://doi.org/10.1016/j.enganabound.2017.09.009

[12] K.H. Kim, G.H. Yoon, Optimal rigid and porous material distributions for noise barrier by acoustic topology optimization, *Journal of Sound and Vibration*, Vol. 339, pp. 123–142, 2015. https://doi.org/10.1016/j.jsv.2014.11.030

[13] K.M. Li, Q. Wang, A bem approach to assess the acoustic performance of noise barriers in a refracting atmosphere, *Journal of Sound and Vibration*, Vol. 211, No. 4, pp. 663–681, 1998. https://doi.org/10.1006/jsvi.1997.1427

[14] P.K. Banerjee, S. Ahmad, H.C. Wang, A new BEM formulation for the acoustic eigenfrequency analysis, *International Journal for Numerical Methods in Engineering,* Vol. 26, No. 6, pp. 1299–1309, 1988. https://doi.org/10.1002/nme.1620260606

[15] A.H. Cheng, D.T. Cheng, Heritage and early history of the boundary element method, *Engineering Analysis with Boundary Elements*, Vol. 29, No. 3, pp. 268–302, 2005. https://doi.org/10.1016/j.enganabound.2004.12.001

[16] L.L. Chen, R.H. Cheng, S.Z. Li, H. Lian, C.J. Zheng, S.P.A. Bordas, A sample-efficient deep learning method for multivariate uncertainty qualification of acoustic–vibration interaction problems, *Computer Methods in Applied Mechanics and Engineering*, Vol. 393,

No.5, Article ID 114784, 2022. https://doi.org/10.1016/j.cma.2022.114784

[17] L.L. Chen, H. Lian, Z. Liu, Y. Gong, C.J. Zheng, S.P.A. Bordas, Bi-material topology optimization for fully coupled structural-acoustic systems with isogeometric FEM–BEM, *Engineering Analysis with Boundary Elements*, Vol. 135, No. 1, pp. 182-195, 2022.

https://doi.org/10.1016/j.enganabound.2021.11.005

[18] L.L. Chen, Z.W. Wang, X. Peng, J.F. Yang, P.F. Wu, H. Lian, Modeling pressurized fracture propagation with the isogeometric BEM, *Geomechanics and Geophysics for Geo-Energy and Geo-Resources,* Vol. 7, No. 51, 2021. https://doi.org/10.1007/s40948-021-00248-3

[19] L.L. Chen, Y. Zhang, H. Lian, E. Atroshchenko, C. Ding, S.P.A. Bordas, Seamless integration of computer-aided geometric modeling and acoustic simulation: Isogeometric boundary element methods based on Catmull-Clark subdivision surfaces, *Advances in Engineering Software*, Vol. 149, Article ID 102879, 2020.

https://doi.org/10.1016/j.advengsoft.2020.102879

[20] Y.J. Liu, On the BEM for acoustic wave problems, *Engineering Analysis with Boundary Elements,* Vol. 107, pp. 53–62, 2019.

https://doi.org/10.1016/j.enganabound.2019.07.002

[21] X.Y. Chen, L. Yao, R.H. Cheng, X.H. Yuan, Y.M. Xu, Sensitivity Analysis for Coupled Structural-Acoustic System with Absorbing Material Using FEM/BEM, *International Journal for Engineering Modelling*, Vol. 34, No. 1, pp. 49–66, 2021.

https://doi.org/10.31534/engmod.2021.1.ri.04f

[22] W.L. Meyer, W.A. Bell, B.T. Zinn, M.P. Stallybrass, Boundary integral solutions of three dimensional acoustic radiation problems, *Journal of Sound and Vibration*, Vol. 59, No. 2, pp. 245–262, 1978. https://doi.org/10.1016/0022-460X(78)90504-7

[23] L.A. de Lacerda, L.C. Wrobel, H. Power, W.J. Mansur, A novel boundary integral formulation for three-dimensional analysis of thin acoustic barriers over an impedance plane, *The Journal of the Acoustical Society of America*, Vol. 104, No. 2, pp. 671–678, 1998.

https://doi.org/10.1121/1.423342

[24] A.F. Seybert, T.K. Rengarajan, The use of CHIEF to obtain unique solutions for acoustic radiation using boundary integral equations, *The Journal of the Acoustical Society of America*, Vol. 81, No. 5, pp. 1299–1306, 1987. https://doi.org/10.1121/1.394535

[25] L.L. Chen, C. Lu, H. Lian, Z.W. Liu, W.C. Zhao, S.Z. Li, H. Chen, S.P.A. Bordas, Acoustic topology optimization of sound absorbing materials directly from subdivision surfaces with isogeometric boundary element methods, *Computer Methods in Applied Mechanics and Engineering*, Vol. 362, No. 3-5, Article ID 112806, 2020.

https://doi.org/10.1016/j.cma.2019.112806

[26] L.L. Chen, H. Lian, S. Natarajan, W. Zhao, X.Y. Chen, S.P.A. Bordas, Multi-frequency acoustic topology optimization of sound-absorption materials with isogeometric boundary element methods accelerated by frequency-decoupling and model order reduction techniques, *Computer Methods in Applied Mechanics and Engineering*, Vol. 395, No. 4, Article ID 114997, 2022. https://doi.org/10.1016/j.cma.2022.114997

[27] S. Li, An efficient technique for multi-frequency acoustic analysis by boundary element method, *Journal of Sound and Vibration*, Vol. 283, No. 3-5, pp.971–980, 2005.

https://doi.org/10.1016/j.jsv.2004.05.027

[28] L.L Chen, C.J. Zheng, H.B. Chen, A wideband FMBEM for 2D acoustic design sensitivity analysis based on direct differentiation method, *Computational Mechanics,* Vol. 52, No.3,

pp. 631–648, 2013. https://doi.org/10.1007/s00466-013-0836-9

[29] C. Vanhille, A. Lavie, An Efficient Tool for Multi-Frequency Analysis in Acoustic Scattering or Radiation by Boundary Element Method, *Acta Acustica united with Acustica*, Vol. 84, No. 5, pp. 884–893, 1998.

[30] T.W. Wu, W.L. Li, A.F. Seybert, An efficient boundary element algorithm for multi-frequency acoustical analysis, *The Journal of the Acoustical Society of America*, Vol. 94, No. 1, pp. 447–452, 1993. https://doi.org/10.1121/1.407056

[31] O.V. Estorff, O. Zaleski, Efficient acoustic calculations by the BEM and frequency interpolated transfer functions, *Engineering Analysis with Boundary Elements*, Vol. 27, No. 7, pp. 683–694, 2003. https://doi.org/10.1016/S0955-7997(03)00023-7

[32] S.T. Raveendra, An efficient indirect boundary element technique for multi-frequency acoustic analysis, *International Journal for Numerical Methods in Engineering*, Vol. 44, No. 1, pp. 59–76, 1999.

https://doi.org/10.1002/(SICI)1097-0207(19990110)44:1<59::AID-NME492>3.0.CO;2-#

[33] J.P. Coyette, C. Lecomte, J.L. Migeot, J. Blanche, M. Rochette, G Mirkovic, Calculation of Vibro-Acoustic Frequency Response Functions Using a Single Frequency Boundary Element Solution and a padé Expansion, *Acta Acustica united with Acustica*, Vol. 85, No. 3, pp. 371–377, 1999.

[34] Z. Wang, Z.G. Zhao, Z.X. Liu, Q.B. Huang, A method for multi-frequency calculation of boundary integral equation in acoustics based on series expansion, *Applied Acoustics*, Vol. 70, No. 3, pp. 459–468, 2009. https://doi.org/10.1016/j.apacoust.2008.05.005

[35] A.J. Burton, G.F. Miller, The application of integral equation methods to the numerical solution of some exterior boundary-value problems, *Physical and Engineering Scien*ces, Vol. 323, No. 1553, pp. 201–210, 1971. https://doi.org/10.1098/rspa.1971.0097

[36] T. Terai, On calculation of sound fields around three dimensional objects by integral equation methods, *Journal of Sound and Vibration,* Vol. 69, No. 1, pp. 71–100, 1980.

https://doi.org/10.1016/0022-460X(80)90436-8

[37] D.F. Paget, The numerical evaluation of Hadamard finite-part integrals, *Numerische Mathematik*, Vol. 36, No. 4, pp. 447–453, 1981. https://doi.org/10.1007/BF01395957

[38] W. Sun, J. Wu, Interpolatory quadrature rules for Hadamard finite-part integrals and their superconvergence, *IMA Journal of Numerical Analysis*, Vol. 28, No. 3, pp. 580–597, 2007. https://doi.org/10.1093/imanum/drm037

[39] E.A. Galapon, The Cauchy principal value and the Hadamard finite part integral as values of absolutely convergent integrals, *Journal of Mathematical Physics,* Vol. 57, No. 3, Article ID 033502,2016. https://doi.org/10.1063/1.4943300

[40] M. Guiggiani, G. Krishnasamy, T.J. Rudolphi, F.J. Rizzo, A General Algorithm for the Numerical Solution of Hypersingular Boundary Integral Equations, *Journal of Applied Mechanics*, Vol. 59, No. 3, pp. 604-614, 1992. https://doi.org/10.1115/1.2893766

[41] J.J. do Rego Silva, *Acoustic and Elastic Wave Scattering Using Boundary Elements*, WIT Press, 1994.

[42] J. Rong, L. Wen, J. Xiao, Efficiency improvement of the polar coordinate transformation for evaluating BEM singular integrals on curved elements, *Engineering Analysis with Boundary Elements,* Vol. 38, pp. 83-93, 2014.

https://doi.org/10.1016/j.enganabound.2013.10.014

[43] S. Keuchel, N.C. Hagelstein, O. Zaleski, O. von Estorff, Evaluation of hypersingular and

nearly singular integrals in the Isogeometric Boundary Element Method for acoustics, *Computer Methods in Applied Mechanics and Engineering*, Vol. 325, pp. 488-504, 2017.

https://doi.org/10.1016/j.cma.2017.07.025

[44] L.L. Chen, H. Lian, Z. Liu, H.B. Chen, E. Atroshchenko, S.P.A. Bordas, Structural shape optimization of three dimensional acoustic problems with isogeometric, *Computer Methods in Applied Mechanics and Engineering*, Vol. 355, pp. 926–951, 2019. https://doi.org/10.1016/j.cma.2019.06.012

[45] Y. Liu, F.J. Rizzo, A weakly singular form of the hypersingular boundary integral equation applied to 3-D acoustic wave problems, *Computer Methods in Applied Mechanics and Engineering*, Vol. 96, No. 2, pp. 271–287, 1992.

https://doi.org/10.1016/0045-7825(92)90136-8

[46] T. Matsumoto, C.J. Zheng, S. Harada, T. Takahashi, Explicit Evaluation of Hypersingular Boundary Integral Equation for 3-D Helmholtz Equation Discretized with Constant Triangular Element, *Journal of Computational Science and Technology*, Vol. 4, No. 3, pp. 194–206, 2010. https://doi.org/10.1299/jcst.4.194

[47] S. Li, Q. Huang, A fast multipole boundary element method based on the improved Burton-Miller formulation for three-dimensional acoustic problems, *Engineering Analysis with Boundary Elements*, Vol. 35, No.5, pp. 719–728, 2011.

https://doi.org/10.1016/j.enganabound.2010.12.004

[48] S. Marburg, The Burton and Miller Method: Unlocking Another Mystery of Its Coupling Parameter, *Journal of Computational Acoustics*, Vol. 24, No. 01, Article ID 1550016, 2016.

https://doi.org/10.1142/S0218396X15500162

[49] L.L. Chen, C. Liu, W.C. Zhao, L.C. Liu, An isogeometric approach of two dimensional acoustic design sensitivity analysis and topology optimization analysis for absorbing material distribution, *Computer Methods in Applied Mechanics and Engineering*, Vol. 336, pp. 507–532, 2018. https://doi.org/10.1016/j.cma.2018.03.025

[50] T. Moller, R. Machiraju, K. Mueller, R. Yagel, Evaluation and design of filters using a Taylor series expansion, *IEEE Transactions on Visualization and Computer Graphics*, Vol. 3, No. 2, pp. 184–199, 1997. https://doi.org/10.1109/2945.597800

[51] Y. Ren, B. Zhang, H. Qiao, A simple Taylor-series expansion method for a class of second kind integral equations, *Journal of Computational and Applied Mathematics*, Vol. 110, No. 1, pp. 15–24, 1999. https://doi.org/10.1016/S0377-0427(99)00192-2

[52] H. Zhou, Y. Liu, J. Wang, Optimizing orthogonal-octahedron finite-difference scheme for 3D acoustic wave modeling by combination of Taylor-series expansion and Remez exchange method, *Exploration Geophysics*, Vol. 52, No. 3, pp. 335–355, 2021.

https://doi.org/10.1080/08123985.2020.1826890

[53] C.J. Zheng, T. Matsumoto, T. Takahashi, H.B. Chen, Explicit evaluation of hypersingular boundary integral equations for acoustic sensitivity analysis based on direct differentiation method, *Engineering Analysis with Boundary Elements,* Vol. 35, No. 11, pp. 1225–1235, 2011. https://doi.org/10.1016/j.enganabound.2011.05.004

[54] M. Junger, D. Feit, *Sound, Structures, and Their Interaction*, The MT Press, 1986.